FE-SEM visualization of cortical microtubules in plant cells using freeze-fracture techniques

Tomohiro Hatano
JEOL Ltd.
Satoshi Nakaba
Tokyo University of Agriculture and Technology
Hikaru Nagata
Tokyo University of Agriculture and Technology
Iwao Doi
Tokyo University of Agriculture and Technology
Yoshiki Horikawa
Tokyo University of Agriculture and Technology
Satoshi Kimura
Tokyo University
Ryo Funada
funada@cc.tuat.ac.jp

Tokyo University of Agriculture and Technology

Method Article

Keywords: Cortical microtubules, Cryo-SEM, FE-SEM, Freeze-fracture, Plant cell wall

Posted Date: January 7th, 2026

DOI: https://doi.org/10.21203/rs.3.rs-8437880/v1

Additional Declarations: No competing interests reported.

Version of Record: A version of this preprint was published at Plant Methods on March 4th, 2026. See the published version at https://doi.org/10.1186/s13007-026-01510-z.

Title: FE-SEM visualization of cortical microtubules in plant cells using freeze-fracture techniques

Authors:

Tomohiro Hatano[1, 2)], Satoshi Nakaba[2, 3)], Hikaru Nagata[2)], Iwao Doi[2)], Yoshiki Horikawa[2, 3)], Satoshi Kimura[4)] and *Ryo Funada[2)]

[1)]JEOL Ltd., Musashino, Akishima, Tokyo, 196-8558, Japan

[2)]Faculty of Agriculture, Tokyo University of Agriculture and Technology, Saiwai-cho, Fuchu, Tokyo, 183-8509, Japan

[3)]Institute of Global Innovation Research, Tokyo University of Agriculture and Technology, Harumi-cho, Fuchu, Tokyo, 183-8538, Japan

[4)]Graduate School of Agricultural and Life Sciences, Tokyo University, Yayoi, Bunkyo-ku, Tokyo, 113-0032, Japan

Corresponding author:

*Ryo Funada

funada@cc.tuat.ac.jp

Abstract

Background

Cortical microtubules (CMTs), one of the components of cytoskeleton, control the orientation and localization of newly deposited cellulose microfibrils in cell walls, and thereby determine the shape, size, and structure of plant cells. Imaging of CMTs in plant tissues is generally performed using fluorescently labeled specimens under an optical fluorescence or confocal laser scanning microscope. However, optical microscopy has insufficient resolution to visualize individual CMTs, and its observation range is limited to superficial tissue layers that light can penetrate. In contrast, transmission electron microscopy offers high-resolution visualization of CMTs in plant cells but is restricted to slightly oblique ultrathin sections with an approximate thickness of 70–100 nm.

Results

Herein, we introduce a technique for visualizing CMTs within unstained plant tissues by combining cryofracture techniques with field emission scanning electron microscopy (FE-SEM). We successfully observed the arrangement of CMTs in several plant specimens, including young branches of ginkgo (*Ginkgo biloba*), calli from the leaves of hybrid poplar (*Populus sieboldii* × *P. grandidentata*), and root tips of the adzuki bean (*Vigna angularis*). CMTs were visualized on the protoplasmic fracture face using both cryo-FE-SEM and conventional room-temperature FE-SEM.

Conclusions

The combination of freeze-fracture techniques with FE-SEM enables the visualization of CMT arrangement in plant tissues at a high resolution and across a broad area without the need for staining or extraction of cellular components. This technique is applicable to various plant tissues and allows for detailed observation of CMTs within these tissues,

providing valuable insights into the role of microtubules in the division and differentiation of plant cells.

Keywords

Cortical microtubules, Cryo-SEM, FE-SEM, Freeze-fracture, Plant cell wall

Introduction

The morphogenesis of plant tissues depends on the orientation and localization of newly deposited cellulose microfibrils (CMFs) on the innermost surface of the primary wall during cell differentiation, which reinforces the cell walls, resulting in resistance to cell expansion in response to turgor pressure[1]. In addition, the orientation of cellulose microfibrils in the secondary walls is closely related to the physical properties of plant cells. The precise control of morphogenesis is crucial for the physical properties of each plant tissue and is essential for the full expression of their functions[2]. Cortical microtubules (CMTs), one of the components of the cytoskeleton, present beneath the

60 plasma membrane regulate the arrangement of CMFs by guiding the movement of
61 cellulose synthase complexes in the plasma membrane in a wide variety of plant cells[3–7].
62 Additionally, CMTs regulate the deposition of non-cellulosic cell wall components by
63 triggering the release of exocytic vesicles[8, 9]. In interphase plant cells, CMTs assemble
64 into highly organized bundles that regulate the direction of cell elongation[10]. The spatial
65 organization of CMT bundles is also believed to play a significant role in the formation
66 of vascular elements with unique cell wall patterns[11, 12]. Thus, a detailed study of CMTs
67 is important in the broader field of plant research, highlighting the need for techniques
68 that allow researchers to visualize CMTs within plant tissues[13].

69 CMTs are fine structures, with a diameter of approximately 25 nm[14], and bundles of
70 microtubules are generally aligned at a close distance of approximately 25 nm[15].
71 Therefore, transmission electron microscopy (TEM), which is capable of high-resolution
72 imaging, has been a useful tool for detailed observations of CMT bundles and of the
73 interactions between their components[13] since the original observations of CMTs in plant
74 cells by Ledbetter and Porter (1963)[16]. However, TEM involves many steps for specimen
75 preparation, including chemical or rapid-freeze fixation, dehydration, and resin
76 embedding, which might introduce artifacts. Additionally, its range of observation is

77 extremely limited because it requires slightly oblique sections of cell membrane,
78 approximately 70–100 nm in thickness, to visualize CMTs[5].

79 With the successful introduction of indirect immunofluorescence staining and confocal
80 laser scanning or fluorescence microscopy for examining much thicker (approximately
81 40 μm) sections than those suitable for TEM, obtaining 3-D images of microtubules over
82 a relatively large area within several plant tissues such as trees has become possible[6, 17–
83 25]. However, owing to limitations of resolution, detailed observation of higher-order CMT
84 arrays using airyscan confocal laser scanning microscopy and structured illumination
85 microscopy would be challenging[26, 27]. Interferometric photoactivation and localization
86 microscopy (iPALM) has successfully been used to measure the diameter of microtubules,
87 approximately 25 nm, by employing fluorescently labeled α-tubulin[28]. However, super-
88 resolution microscopy techniques are sensitive to autofluorescent molecules, which
89 makes them unsuitable for plant cells with abundant pigments and phenolic compounds[13].
90 Therefore, for the precise visualization of CMTs in a wide variety of plant cells, technical
91 advances are needed[13, 29, 30].

92 Here, we report a novel method for intact and high-resolution observation of CMT arrays

93 across a wide area in different plant, cells by combining a rapid plunge-freezing technique,
94 freeze-fracture equipment, and field emission scanning electron microscopy (FE-SEM).
95 Microtubules within plant tissues have previously been observed using FE-SEM[31-35].
96 However, pretreatment with chemical fixation and extraction of cellular components is
97 needed, which potentially leads to the possibility of artifacts during preparation. In
98 contrast, TEM analysis of replica membranes using a freeze-fracture device has yielded
99 significant findings in studies of membrane proteins in plant cells[36, 37] . However, freeze-
100 replica techniques show an overestimation of structures due to the deposition of carbon
101 and platinum films and the loss of positional information during the collection of the
102 replica membrane. In contrast, our method, which uses a freeze-fracture technique,
103 eliminates the need for creating a replica membrane and chemical fixation and dissolution
104 procedures, allowing for direct observation of cellular microstructures. Additionally, FE-
105 SEM enables seamless high-resolution observations across a wide range of
106 magnifications in plant cells[38], providing detailed insights into the higher-order
107 arrangement of CMT bundles in plant tissues. In this study, we conducted a comparative
108 examination of the two primary methods of the freeze-fracture technique, namely knife
109 fracture and tensile fracture[39], and used multiple experimental materials to visualize

CMTs in various plant cells.

Results

Cryo-FE-SEM images of freeze-knife–fractured young branches of ginkgo (*Ginkgo biloba*)

Figure 1 presents the terminology used for freeze-fractured faces and surfaces. The fracture face, known as the protoplasmic fracture face (PF) or the exoplasmic fracture face (EF), represents the hydrophobic part of the membrane that is typically exposed by the freeze-fracture process[40]. The protoplasmic surface (PS) or exoplasmic surface (ES) corresponds to the hydrophilic part of the membrane, and is usually revealed through a sublimation process[40].

Figure 2 shows cryo-FE-SEM images of young branches of *G. biloba*. Figures 2A-D show the freeze-knife–fractured faces of regions in the phloem axial parenchyma cells. On the exposed PF, numerous CMTs oriented nearly perpendicular to the direction of cell elongation could be observed (Fig. 2C). These CMTs exhibited a meandering

arrangement in the cytoplasm, with some oriented almost parallel to the direction of cell elongation. In this region, although a few CMTs formed bundles, most were arranged individually. When CMTs were bundled, ladder-like structures connecting the microtubules were observed (Fig. 2D). Figures 2E-F show the freeze-knife–fractured face of the epidermal parenchyma cells in young branches of *G. biloba*. CMT bundles oriented at an angle of approximately 45° to the direction of cell elongation were observed at the PF (Fig. 2E-F). Each bundle consisted of 3–4 CMTs, and a few CMTs existed individually. These CMTs were linearly arranged in the cytoplasm, with no meandering microtubules.

Cryo-FE-SEM images of freeze-knife–fractured calli of hybrid poplar (*Populus sieboldii* × *P. grandidentata*)

Figure 3 shows cryo-FE-SEM images of the calli of hybrid poplar (*Populus sieboldii* × *P. grandidentata*). In the exposed PF region, the cell surface exhibited a smooth dome-like shape (Fig. 3A). In the PF, CMTs were oriented nearly perpendicular to the longitudinal axis of the cells, which corresponded to the direction of cell elongation (Fig. 3B). Most CMTs were bundled, although some existed as individual units. In

141 regions where CMTs were densely bundled, each CMT bundle consisted of 4–6
142 microtubules (Fig. 3C). Beneath the CMTs, organelles presumed to be mitochondria
143 were observed in the cytoplasm (Fig. 3B).

144

145 **Cryo-FE-SEM images of freeze-tensile–fractured face of root tips of adzuki beans**
146 **(*Vigna angularis*)**

147 Figure 4 shows cryo-FE-SEM images of a freeze-tensile–fractured face of the root tips
148 of adzuki bean (*Vigna angularis*). The PF and exoplasmic fracture face (EF) were
149 reproducibly observed at the sites where separation occurred between the lipid bilayers
150 (Fig. 4A and B). Island-like depressions were present on the EF because of the partial
151 absence of the cell membrane (Fig. 4B and D). Although difficult to identify in the cryo-
152 FE-SEM image, detached ES was easily observed partially adhering to the PF after
153 freeze substitution (FS) and critical point drying (CPD), as described later. On the PF,
154 CMTs were oriented approximately perpendicular to the direction of cell elongation
155 (Fig. 4C, Fig. 5). The diameters of the CMTs in *V. angularis* were greater than those in
156 the young branches of *G. biloba* and calli from the hybrid poplar (*Populus sieboldii* × *P.*

157 *grandid*). In areas where the cell membrane was absent in the EF, CMFs were exposed
158 (Fig. 4D). The orientations of the CMFs and CMTs were nearly identical, aligning
159 approximately perpendicular to the direction of tissue elongation, indicating that CMTs
160 control the orientation of CMFs and, therefore, the cell shape.

161

162 **FE-SEM images captured at room temperature of freeze-tensile–fractured face of**
163 **root tops of adzuki bean (*Vigna angularis*) after freeze substitution and critical**
164 **point drying**

165 Figure 6 shows FE-SEM images of a freeze-tensile–fractured face of root tips of *V.*
166 *angularis* at room temperature (25 °C). The samples were subjected to treatments of FS
167 and CPD. The PF was exposed over a wide area in the region fractured between the
168 lipid bilayers (Fig. 6C and D). The EFs in the cryo-FE-SEM images (Fig. 4A and B)
169 were not observed in the samples after treatment with FS and CPD. The CMTs that were
170 oriented approximately perpendicular to the direction of cell elongation were observed
171 in the PF (Fig. 6E and Fig. 7). The surfaces of CMTs appeared to be covered with the
172 protoplasmic half (P half) of the lipid bilayer and a tissue-derived extract. The diameters

173 of these CMTs were greater than those of the ginkgo and hybrid poplar calli (*Populus*
174 *sieboldii* × *P. grandidentata*). Although some CMTs were bundled together, they
175 appeared to exist individually. ESs, with diameters of several hundred nanometer, were
176 also observed in some regions, exhibiting an island-like shape on the PF.

177

178 **Discussion**

179 In this study, we demonstrated that the arrangement of CMTs could be visualized at
180 high resolution by rapidly freezing the samples and performing high-resolution FE-
181 SEM observations of freeze-fractured faces.

182

183 **Cryo-FE-SEM observations**

184 During the freeze-fracture process, cracks are formed between the lipid bilayers of the
185 cell membrane, exposing the EF and PF[41]. In the freeze-fracture replica method, which
186 involves vacuum deposition of Pt and C, membrane proteins are observed in the PF[39]. In
187 contrast, because our method did not involve vacuum deposition, we observed CMTs

188 located beneath the cell membrane (Figs. 2–7). The escape depth of secondary electrons
189 is within 10 nm of the outermost surface of the samples[42]; therefore, secondary electron
190 images obtained using SEM primarily provide information about the outermost surface
191 of the samples. However, because the P half of the lipid bilayer is estimated to be
192 several nanometers thick, CMTs located beneath the PF could be observed using FE-
193 SEM. The CMTs observed using FE-SEM in this study, as well as in previous studies,
194 had slightly larger diameters than those observed using TEM (Figs. 2–7)[31, 35]. These
195 differences were particularly noticeable in CMTs of young branches of *G. biloba*. In
196 cryo-FE-SEM observations, any frost or ice that adheres during transportation is
197 sublimated in the high vacuum of the FE-SEM device before observation. As ice formed
198 from water between the cytoplasm and cell membrane sublimates, the P half of the lipid
199 bilayer is presumed to cover the CMTs on the PF. This attachment of the P half likely
200 contributed to the slight increase in the thickness of CMTs in this study.

201 In addition, we observed cross-linked structures that connected microtubules at
202 consistent distances in the bundled regions of CMTs of young branches of *G. biloba*
203 (Fig. 2D). The microtubule-associated protein MAP65 connects CMTs, maintaining a
204 parallel spacing of 25–30 nm, which appears as filamentous crosslinks in TEM

observations[12]. The crosslinked structures connecting CMTs observed in this study may be CMT-associated proteins (MAPs) that play an important role in maintaining parallelism of CMTs. Because FE-SEM observations using our method reflect the state modified by MAPs, the differences in the diameters of CMTs among the different plant samples might reflect variations in their modification states.

Samples after freeze substitution and critical point drying

The CMTs were also observed using room-temperature FE-SEM after the samples underwent FS and CPD (Fig. 6). Compared with the cryo-FE-SEM images, PF after FS and CPD appeared to have more surface deposits (Fig. 6E-F). This was likely due to components leaking from the plant tissues during the FS process and adhering to the surface of the samples.

The EF fragments that were complementary paired with the PS in cryo-FE-SEM (Fig. 4A and B) were not observed in room-temperature FE-SEM following FS and CPD. As the EF fragments were weakly attached to the sample, most of them might have been lost during FS or CPD. If cryo-FE-SEM is not available, FE-SEM at room temperature

221 after FS and CPD might be effective in observing CMTs. However, this pretreatment
222 might lead to an increase in the amounts of deposits on the sample surface.

223

224 **Freeze-knife fracture and freeze-tensile fracture method**

225 The freeze-tensile fracture method produced PF with a larger area than did the freeze-
226 knife fracture method. This approach allowed the observation of both sides of the PF
227 and EF, which are complementary (Fig. 4A and B). In addition, by excising a specific
228 area of interest, sandwiching it between copper plates, and then peeling it off, this
229 method enables the observation of CMTs within the interior of plant tissues,
230 demonstrating an additional advantage.

231 In cross-sections prepared using the freeze-tensile fracture method, island-like
232 fragments of the ES were observed on the PF (Fig. 6E and F). However, no such island-
233 like ES fragments were observed on freeze-knife-fractured faces (Figs. 2 and 3).
234 Therefore, the island-shaped ES fragments, which resisted the freeze-tensile process,
235 might correspond to lipid rafts where membrane proteins accumulate.

The cross-sections prepared via the freeze-knife fracture and freeze-tensile fracture methods were highly cracked between lipid bilayers and exhibited various fracture patterns. Consequently, it is difficult to selectively observe the CMTs in specific regions using these methods. Moreover, because the depth of vitreous ice formation in plunge rapid freezing is limited to approximately 20 μm[43], it is advisable to perform fracturing close to the frozen surface.

Conclusions

Our study demonstrates that the combination of cryofracture techniques with FE-SEM observation is effective for the high-resolution imaging of fine CMTs in plant tissues. This method is applicable to various plant tissues and is particularly useful for visualizing CMTs within plant tissues that are challenging to observe with an optical microscope. In contrast, it is important to note that when using our method, the CMTs are covered by the P half of the thin cell membranes at the nanoscale, and the freeze-fractured cross-sections can display various fracture patterns. Therefore, careful consideration is needed when interpreting FE-SEM images of CMTs.

252

253 **Methods**

254 The materials used in this study were young branches of *G. biloba* growing on the campus
255 of Tokyo University of Agriculture and Technology in Fuchu, Tokyo, calli derived from
256 leaves of hybrid poplar (*P. sieboldii* × *P. grandidentata*) growing on the same campus[44],
257 and root tips of *V. angularis* (adzuki bean; commercial Tamba Dainagon) approximately
258 one week after sowing.

259

260 **Plunge freezing**

261 An aluminum metal cup was cooled to liquid nitrogen temperature and filled with ethane
262 gas (99.5% purity; GL Sciences, Tokyo, Japan) to produce liquefied ethane. The
263 cryoembedding medium was prepared using bovine albumin (FUJIFILM Wako Pure
264 Chemical Corporation, Osaka, Japan) dissolved in four-volumes of distilled water. The
265 samples were secured by applying a thin layer of bovine albumin solution to the sample
266 stage during rapid freezing. Young branches of *G. biloba* and calli derived from the

267 petioles of hybrid poplar (*P. sieboldii* × *P. grandidentata*) used in the freeze-knife fracture
268 experiments were cut into pieces several millimeters in length and positioned on a copper
269 hat-type sample stage for the freeze-fracture device. Rapid freezing was performed by
270 immersing the sample in liquid ethane while being fixed on the sample stage. The root
271 tips of *V. angularis* used in the freeze-tensile fracture experiments were sliced to a
272 thickness of several hundred micrometers with a razor and then securely placed between
273 two copper disks (0.1 mm thick, approximately 3 mm in diameter, Nisshin EM, Tokyo,
274 Japan). The sample sandwiched between the copper disks was rapidly frozen by pinching
275 with tweezers and immersing in liquid ethane[45]. The frozen samples were then attached
276 to the sample stage of the freeze-fracture device and stored in liquid nitrogen.

277

278 **Freeze-fracture and cryo-FE-SEM observations**

279 The frozen samples were placed into a freeze-fracture device (EM-19501JFDV, JEOL,
280 Tokyo, Japan) for freeze-knife fracture and freeze-tensile fracture at a sample stage
281 temperature of −110 °C and a knife temperature of −180 °C. Young branches of *G. biloba*
282 and calli of hybrid poplar (*P. sieboldii* × *P. grandidentata*) were freeze-fractured a few

283 micrometers from the outermost surface of the specimen using a knife attached to a
284 freeze-fracture device. The freeze-tensile fracture process for the root tips of *V. angularis*
285 was performed by removing the copper plate from the sample using a knife attached to
286 the freeze-fracture device. The samples remaining on the copper disk above the sample
287 stage after the tensile fracture were used for SEM observations. After freeze-fracturing,
288 the samples were stored in liquid nitrogen and inserted into the FE-SEM (JSM-7100F,
289 JEOL) equipped with a cryo-unit (MP-Z08181T, JEOL). Cryo-FE-SEM observations
290 were carried out at an accelerating voltage of 1 kV and a sample stage temperature of
291 −90 °C. Images were captured using a secondary electron detector. Before observation,
292 any frost that accumulated during the transportation of the sample was sublimated within
293 the cryo-FE-SEM device. No conductive coating was applied for the cryo-FE-SEM
294 observations.

295

296 **Freeze substitution and critical point drying**

297 FS was performed by immersing the freeze-tensile fractured root tips of *V. angularis* in
298 2% OsO_4 in acetone and storing them at −85 °C for 2 days, at −20 °C for 4 h, and at 4 °C

for 2 h. The samples were then warmed to 25 °C and washed several times with 100% acetone. The samples were placed in a critical point dryer (SYSGLCP-8; Sanyu-Gijutsu, Tokyo, Japan). CPD was carried out at a flow rate of 1.0 L/min and a temperature of 40 °C. After CPD, the samples were coated with a 1.5 nm-thick layer of osmium using an osmium plasma coater (HPC-20; Vacuum Device, Ibaraki, Japan). Observations were made using an FE-SEM device (JSM-7900F, JEOL) at an accelerating voltage of 1 kV, and the images were acquired using a secondary electron detector.

Abbreviations

CPD: critical point drying

CMFs: cellulose microfibrils

CMT: cortical microtubule

EF: endoplasmic fracture face

E half: exoplasmic half

313 ES: exoplasmic surface

314 FE-SEM: field emission scanning electron microscopy

315 FS: freeze-substitution

316 PF: protoplasmic fracture face

317 P half: protoplasmic half

318 PS: protoplasmic surface

319 TEM: transmission electron microscopy

320

321 **Data availability**

322 All image data are available in the main text.

323

324 **References**

325 1. Seagull RW. Role of the cytoskeletal elements in organized wall microfibril deposition.

In: Haigler CH, Weimer PJ, editors. Biosynthesis and biodegradation of cellulose. Marcel Dekker; 1990. pp. 143-164.

2. Panteris E, Galatis B. The morphogenesis of lobed plant cells in the mesophylland epidermis: organization and distinct roles of cortical microtubules and actin filaments. New Phytol. 2005; 167: 721–732.

3. Elliott A, Shaw SL. Update: Plant cortical microtubule arrays. Plant Physiol. 2018; 176: 94–105.

4. Paredez AR, Somerville CR, Ehrhardt DW. Visualization of cellulose synthase demonstrates functional association with microtubules. Science. 2006; 312: 1491–1495.

5. Chaffey N. Conventional (chemical fixation) transmission electron microscopy and cytochemistry of angiosperm trees. In: Chaffey N, editor. Wood formation in trees: cell and molecular biology techniques. Taylor and Francis; 2001. pp. 41–64.

6. Funada R. Immunolocalisation and visualisation of the cytoskeleton in gymnosperms using confocal laser scanning microscopy (CLSM). In: Chaffey N, editor. Wood formation in trees: cell and molecular biology techniques. Taylor and Francis; 2001.

342 pp. 143–157.

343 7. Funada R. Microtubules and the control of wood formation. In: Nick P, editor. Plant
344 microtubules: development and flexibility. Springer-Verlag; 2008. pp. 83–119.

345 8. Zhu C, Ganguly A. Baskin TI, McClosky DD, Anderson CT, Foster C, et al. The fragile
346 fiber1 kinesin contributes to cortical microtubule-mediated trafficking of cell wall
347 components. Plant Physiol. 2015; 67: 780–792.

348 9. Oda Y. Cortical microtubule rearrangements and cell wall patterning. Front Plant Sci.
349 2015; 6: 236.

350 10. Wasteneys GO, Ambrose JC. Spatial organization of plant cortical microtubules:
351 close encounters of the 2D kind. Trends Cell Biol. 2009; 19: 62-71.

352 11. Derbyshire P, Menard D, Green P, Saalbach G, Buschman H, Loyd CW, et al.
353 Proteomic analysis of microtubule interacting proteins over the course of xylem
354 tracheary element formation in Arabidopsis. The Plant Cell. 2015; 27: 2709–2726.

355 12. Mao G, Buschmann H, Doonan JH, Lloyd CW. The role of MAP65-1 in microtubule
356 bundling during Zinnia tracheary element formation. J Cell Sci. 2006; 119: 753–758.

357 13. Celler K, Fujita M, Kawamura E, Ambrose C, Haerburger K, Holzinger A et al.

358 Microtubules in plant cells: strategies and methods for immunofluorescence,
359 transmission electron microscopy, and live cell imaging. Methods Mol Biol. 2016;
360 1365: 155–184.

361 14. Ledbetter MC. Porter KR. Morphology of microtubules of plant cell. Science. 1964;
362 144; 872–874.

363 15. Tulin A, McClerklin S, Huang Y, Dixit R. Single-molecule analysis of the
364 microtubule cross-linking protein MAP65-1 reveals a molecular mechanism
365 forcontact-angle-dependent microtubule bundling. Biophys J. 2012; 102: 802–809.

366 16. Ledbetter M, Porter KR. A “Microtubule” in plant cell fine structure. J Cell Biol;
367 1963; 19: 239–250.

368 17. Uehara K, Hogetsu T. Arrangement of cortical microtubules during formation of
369 bordered pits in the tracheids of *Taxus*. Protoplasma; 1993; 172: 145-153.

370 18. Abe H, Funada R, Imaizumi H, Ohtani J, Fukazawa K. Dynamic changes in the
371 arrangement of cortical microtubules in conifer tracheids during differentiation.
372 Planta. 1995; 197: 418–421.

373 19. Abe H, Funada R, Ohtani J, Fukazawa K. Changes in the arrangement of microtubules

374 and microfibrils in differentiating conifer tracheids during the expansion of cells. Ann
375 Bot. 1995; 75: 305–310.

376 20. Funada R, Abe H, Furusawa O, Imaizumi H, Fukazawa K, Ohtani J. The orientation
377 and localization of cortical microtubules in differentiating conifer tracheids during
378 cell expansion. Plant Cell Physiol. 1997; 38: 210–212.

379 21. Furusawa O, Funada R, Murakami Y, Ohtani J. Arrangement of cortical microtubules
380 in compression wood tracheids of *Taxus cuspidata* visualized by confocal laser
381 microscopy. J Wood Sci. 1998; 44: 230–233.

382 22. Funada R, Miura H, Shibagaki M, Furusawa O, Miura T, Fukatsu E, et al. Involvement
383 of localized cortical microtubules in the formation of a modified structure of wood. J
384 Plant Res. 2001; 114: 491–497.

385 23. Chaffey N. Immunolocalisation of the cytoskeleton in the secondary vascular system
386 of angiosperm trees and its visualization using epifluorescence microscopy. In:
387 Chaffey N, editor. Wood formation in trees: cell and molecular biology techniques.
388 Taylor and Francis; 2001. pp. 113–142.

389 24. Begum S, Furusawa O, Shibagaki M, Nakaba S, Yamagishi Y, Yoshimoto J, et al. Cold

390 stability of microtubules in wood-forming tissues of conifers during seasons of active
391 and dormant cambium. Planta. 2012; 235: 165–179.

392 25. Begum S, Furusawa O, Shibagaki M, Nakaba S, Yamagishi Y, Yoshimoto J, et al.
393 Localization of actin filaments and cortical microtubules in wood-forming tissues of
394 conifers. IAWA J. 2019; 40: 703-720.

395 26. Vavrdová T, Šamajová O, Krenek P, Ovecka M, Šamajová O, Floková P, Illešová P,
396 et al. Multicolor three dimensional structured illumination microscopy of
397 immunolabeled plant microtubules and associated proteins. Plant Methods. 2019; 15:
398 622

399 27. Vavrdová T, Krenek P, Ovecka M, Šamajová O, Floková P, Illešová P, et al.
400 Complementary superresolution visualization of composite plant microtubule
401 organization and dynamics. Front Plant Sci. 2020; 11: 693.

402 28. Shtengel G, Galbraith JA, Galbraith CG, Lippincott-Schwartzd J, Gillette JM, Manley
403 S, et al. Interferometric fluorescent super-resolution microscopy resolves 3D cellular
404 ultrastructure. Proc Natl Acad Sci USA. 2009; 106: 3125–3130.

405 29. Nakaba S, Kitin P, Yamagishi Y, Begum S, Kudo K, Nugroho WD, et al. Three-

406 dimensional imaging of cambium and secondary xylem cells by confocal laser
407 scanning microscopy. In: Yeung ECT, Stasolla C, Summer MJ, Huang BQ, editors.
408 Plant micro techniques and protocols, Springer; 2015. pp. 431-465.

409 30. Park SW, Muroyama A. Technological advances in visualizing and rewiring
410 microtubules during plant development. J Exp Bot. 2026; 77: 51-62.

411 31. Abe H, Ohtani J, Fukazawa KA. Scanning electron microscopic study of changes in
412 microtubule distributions during secondary wall formation in tracheids. IAWA J.
413 1994; 15: 185–189.

414 32. Prodhan AKMA, Funada R, Ohtani J, Abe H, Fukazawa K. Orientation of microfibrils
415 and microtubules in developing tension-wood fibres of Japanese ash (*Fraxinus*
416 *mandshurica* var. *japonica*). Planta. 1995; 196: 577–585.

417 33. Vesk PA, Vesk M, Gunning BES. Field emission scanning electron microscopy of
418 microtubule arrays in higher plant cells. Protoplasma. 1996; 195: 168–182.

419 34. Vesk M, Dibbayawan TP, Vesk PA, Egan EA. Field emission scanning electron
420 microscopy of plant cells. Protoplasma. 2000; 210: 138–155.

421 35. Barton DA, Vantard M, Overall RL. Analysis of cortical arrays from *Tradescantia*

422 *virginiana* at high resolution reveals discrete microtubule subpopulations and
423 demonstrates that confocal images of arrays can be misleading. The Plant Cell. 2008;
424 20: 982–994.

425 36. Kimura S, Laosinchai W, Itoh T, Cui X, Linder R, Brown Jr RM, et al. Immunogold
426 labeling of rosette terminal cellulose-synthesizing complexes in the vascular plant
427 *Vigna angularis*. The Plant Cell. 1999; 11: 2075–2086.

428 37. Itoh T, Kimura S, Brown RM. Immunogold labeling of cellulose-synthesizing
429 terminal complexes. In: Brown RM, Saxena IM, editors. Cellulose: molecular and
430 structural biology. Springer; 2007. pp. 237–255.

431 38. Hatano T, Nakaba S, Horikawa Y, Funada R. A combination of scanning electron
432 microscopy and broad argon ion beam milling provides intact structure of secondary
433 tissues in woody plants. Sci Rep. 2022; 12: 9152.

434 39. Severs NJ. Freeze-fracture electron microscopy. Nature Protocol. 2007; 2: 547–576.

435 40. Branton D, Bullivant S, Gilula NB, Karnovsky MJ, Moor H, Mühlethaler K, et al. Freeze-
436 etching nomenclature. Science. 1975; 190: 54–56.

437 41. Pinto da Silva P, Parkison C, Dwyer N. Fracture-label: O cytochemistry of freeze-

438 fracture faces in the erythrocyte membrane. Proc Natl Acad Sci USA. 1981; 78: 343–
439 347.

440 42. Seiler H. Secondary electron emission in the scanning electron microscope. J Applied
441 Physics. 1983; 54: R1–R18.

442 43. Giddings Jr TH, O'Toole ET, Morphew M, Mastronarde DN, Mclntoshh JR, Winey
443 M, et al. Using rapid freeze and freeze-substitution for the preparation of yeast cells
444 for electron microscopy and three-dimensional analysis. Methods Cell Biol. 2001;
445 67: 27–42.

446 44. Yamagishi Y, Yoshimoto J, Uchiyama H, Nabeshima E, Nakaba S, Watanabe U, et
447 al. In vitro induction of secondary xylem-like tracheary elements in calli of hybrid
448 poplar (*Populus sieboldii* x *P. grandidentata*). Planta. 2013; 237: 1179-1185.

449 45. Yamaguchi M, Wakabayashi S, Nakamura Y, Matsue H, Hirao T, Aoki S, et al. Good
450 ultrastructural preservation of human tissues and cultured cells by glutaraldehyde
451 fixation, sandwich freezing, andfreeze-substitution. Cytologia. 2020; 85: 15–26.

452

453 **Acknowledgements**

We would like to express our sincere gratitude to Professor Emeritus Takao Ito of Kyoto University for his invaluable guidance on preprocessing methodologies and interpretation of experimental data.

Funding

This work was supported, in part, by Grants-in-Aids for Scientific Research from the Japan Society for the Promotion of Science (JSPS) (nos. 18H02251, 21H02253 and 24 K01822).

Contributions

TH, SN, YH, SK, HN, ID, and RF contributed to the study conception and design. TH performed the experiments. TH and RF wrote the manuscript. HN and ID cultivated hybrid poplar calli. All authors read and approved the final manuscript.

Ethics declarations

Ethics approval and consent to participate

Not applicable.

Consent for publication

Not applicable.

Competing interests

The authors declare that they have no competing interests.

Statement of compliance

Plant experiments and the collection of plant materials were performed in accordance with relevant institutional, national, and international guidelines and legislation.

Figures and legends to figures

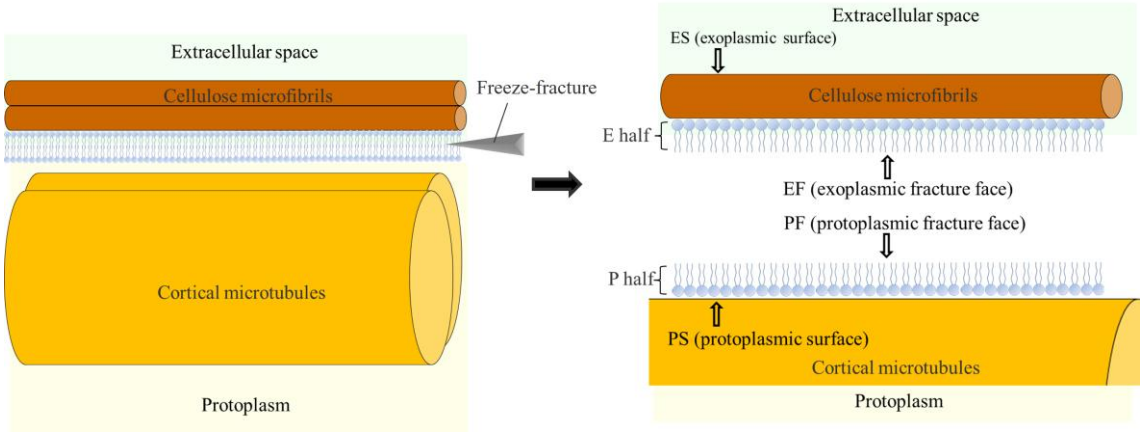

Figure 1. Nomenclature for freeze-fractured faces and surfaces

The fracture face, termed the protoplasmic fracture face (PF) or exoplasmic fracture face (EF), represents the hydrophobic portion of the membrane that is typically exposed during the freeze-fracture process. The protoplasmic surface (PS) or exoplasmic surface (ES) corresponds to the hydrophilic portion of the membrane and is usually revealed through sublimation. E half = exoplasmic half; P half = protoplasmic half.

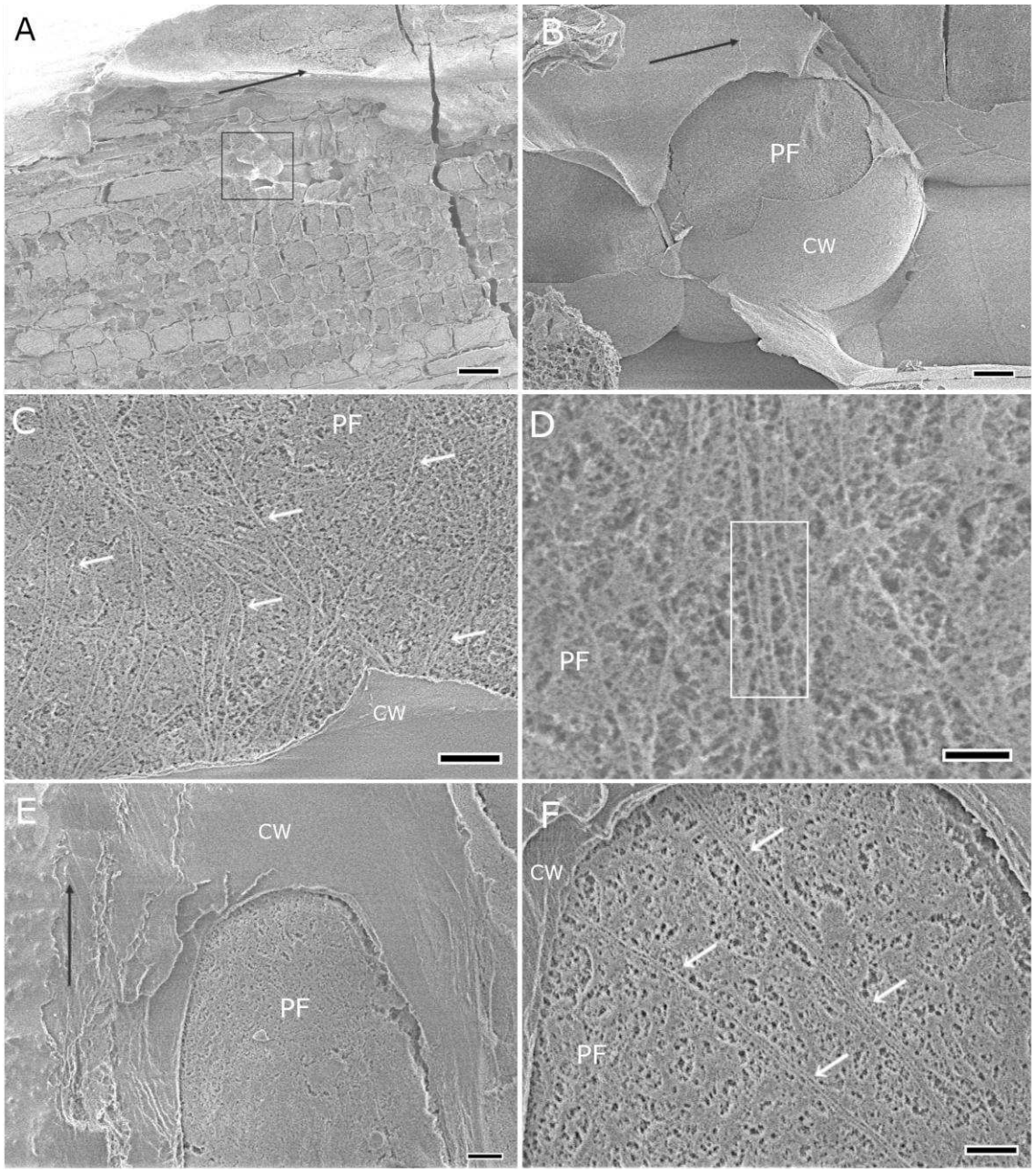

492

493 **Figure 2 Cryo-FE-SEM images of freeze-knife–fractured faces of young branches of**

494 **ginkgo (*Ginkgo biloba*)**

495 Cryo-FE-SEM images of freeze-knife–fractured faces of young branches of gingko (*G.*

biloba). A, B: Low-magnification images. Boxed areas indicate the location of the phloem axial parenchyma cells, as shown in Figure 2 B–D. C: Numerous cortical microtubules (CMTs) were observed on the protoplasmic fracture face (PF) of phloem axial parenchyma cells. The CMTs were generally oriented nearly perpendicular to the direction of cell elongation, with most exhibiting a meandering pattern across the cytoplasm. However, some CMTs were aligned nearly parallel to the direction of elongation. D: High-magnification image of the PF. In regions where CMTs were bundled, ladder-like structures connecting adjacent microtubules were observed (boxed area). E, F: In the PF of the epidermal parenchyma cells, the CMT bundles were arranged at an angle of approximately 45 ° relative to the direction of elongation. Each CMT bundle consisted of 3–4 microtubules.

Black arrows = direction of cell elongation; White arrows = CMTs; CW = cell wall. Scale bars = 50 μm (A), 5 μm (B), 1 μm (C, E), 500 nm (D, F).

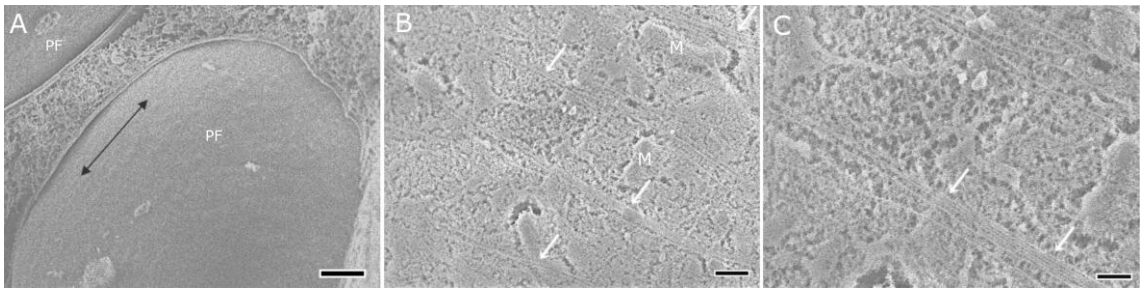

Figure 3 Cryo-FE-SEM images of freeze-knife–fractured calli of hybrid poplar (*Populus sieboldii* × *P. grandidentata*)

Cryo-FE-SEM image of a freeze-knife–fractured face of the calli of hybrid poplar (*P. sieboldii* × *P. grandidentata*). A: The cell surface exhibited a smooth, dome-like shape on the protoplasmic fracture face (PF). B: On the PF, cortical microtubules (CMTs) were aligned nearly perpendicular to the longitudinal axis of the cell. C: In regions where CMTs were densely bundled, each CMT bundle consisted of 4–6 microtubules. Black arrow = longitudinal axis of the cell; White arrows = CMTs; M = mitochondria. Scale bars = 3 μm (A), 1 μm (B), 500 nm (C).

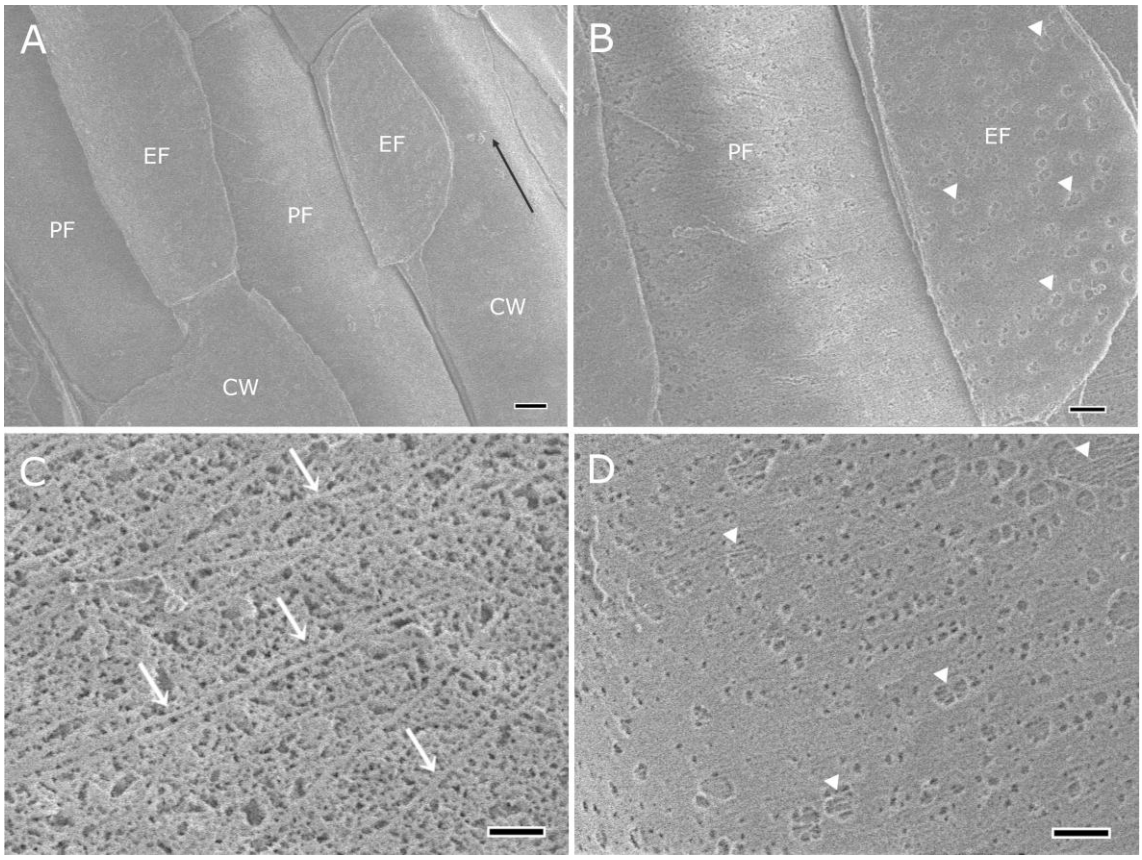

Figure 4 Cryo-FE-SEM image of freeze-tensile–fractured surface of roots tips of adzuki beans (*Vigna angularis*)

Cryo-FE-SEM images of a freeze-tensile–fractured face of the root tips of adzuki bean (*V. angularis*). A, B: Both the protoplasmic fracture face (PF) and exoplasmic fracture face (EF) were reproducibly observed at the interfacial fracture of the lipid bilayer. Island-shaped depressions (white arrowheads) caused by the absence of the cell membrane were formed on the EF. C: High-magnification image of the PF showing numerous cortical microtubules (CMTs) oriented approximately perpendicular to the

direction of cell elongation. Occasionally, CMT bundles consisting of two microtubules were observed. D: Enlarged image of EF shows cellulose microfibrils (CMFs) in areas where the cell membrane was absent (white arrowheads). The orientations of CMFs and CMTs were nearly identical.

Black arrow = direction of cell elongation; White arrows = CMTs; CW = cell wall.

Scale bars = 2 μm (A), 1 μm (B), 500 nm (C, D).

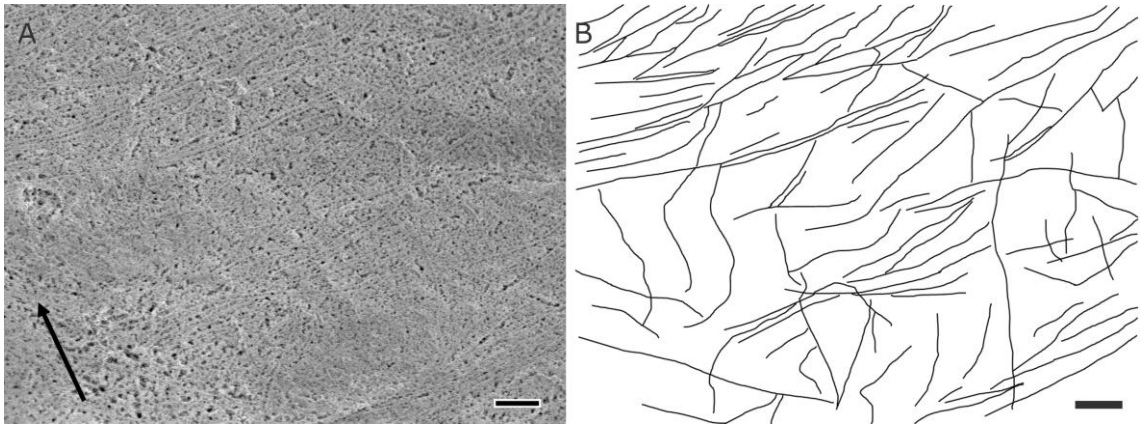

Figure 5 Tracing of cortical microtubules on the protoplasmic fracture face of root tips of adzuki bean (*Vigna angularis*)

A: Cryo-FE-SEM image of the protoplasmic fracture face (PF) from the root tips of adzuki bean (*V. angularis*). B: Tracing of cortical microtubules (CMTs) on the PF, created based on the SEM image shown in Figure 5A. The identification of CMTs was performed via visual confirmation.

Black arrow = direction of cell elongation; Scale bar = 1 μm.

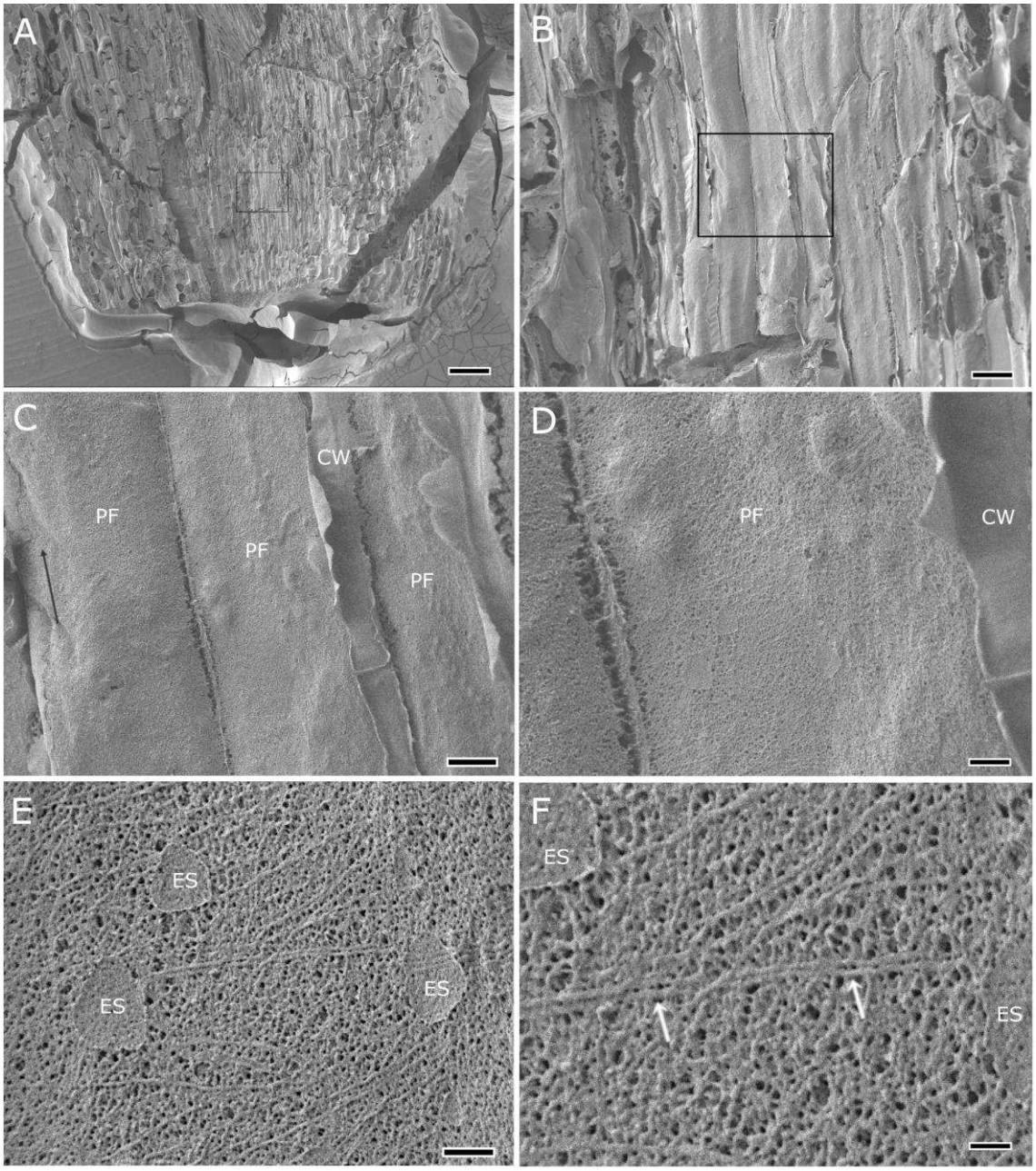

546

547 **Figure 6 FE-SEM images captured at room temperature of freeze-tensile–**

548 **fractured face of root tips of adzuki bean (*Vigna angularis*)**

549 FE-SEM images of a freeze-tensile fractured surface of the root tips of adzuki bean (*V.*

550 *angularis*) captured at room temperature after freeze substitution and critical point

551 drying treatment. A, B: Low-magnification images. The boxed areas indicate the

552 positions of the cells observed at high magnification in Figure 6 C-F. C, D: A

553 widespread protoplasmic fracture face (PF) with numerous cortical microtubules

554 (CMTs). The exoplasmic fracture face (EF), which complementarily pairs with the PF

555 observed via cryo-FE-SEM, was absent. E, F: Enlarged views of the PF. The CMTs

556 were oriented approximately perpendicular to the direction of cell elongation and their

557 surfaces appeared to be covered by the protoplasmic half (P half) of the lipid bilayer.

558 Island-like shapes of the ESs were also observed in some regions.

559 Black arrow = direction of cell elongation; White arrows = CMTs; CW = cell wall.

560 Scale bars = 100 μm (A), 10 μm (B), 3 μm (C), 1 μm (D), 500 nm (E), 200 nm (F).

561

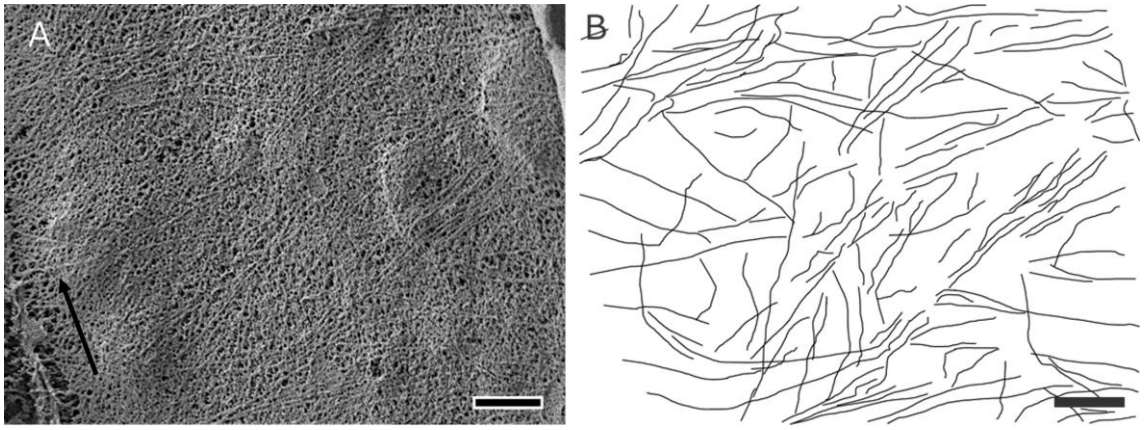

Figure 7 Tracing of cortical microtubules on the protoplasmic fracture face of root tips of adzuki bean (*Vigna angularis*) after freeze substitution and critical point drying treatment

A: FE-SEM image of the protoplasmic fracture face (PF) of the root tips of adzuki bean (*V. angularis*) captured at room temperature. B: Tracing of cortical microtubules (CMTs) on the PF, created based on the SEM image shown in Figure 7A. The identification of CMTs was performed via visual confirmation.

Black arrow = direction of cell elongation; Scale bar = 1 μm.